ICSE-Q 1st International Congress on Surface Engineering / IWTS-Q
June 29th-July 1st 2016

# INFLUENCE OF TUNGSTEN CARBIDE NANO-CRYSTAL PARTICLE ADDITION ON THE HARDFACING PROPERTIES OF NI-BASED ALLOYS

Ali Tahaei[1], Felipe Garcia[2], Mattia Merlin[1], Felipe Arturo Reyes Valdez[2], Gian Luca Garagnani[1], Ana Arizmendi Moquecho[3*]

[1]Department of Engineering, University of Ferrara, Ferrara, Italy
[2]Corporación Mexicana de Investigación en Materiales, Saltillo, Mexico
[3]Cimav-Unidad Monterrey, Monterrey, Nuevo León, Mexico
*ali.tahaei@unife.it

**ABSTRACT**
In this research, a nickel-base powder reinforced with tungsten carbide particles (micron size) was applied by Plasma Transferred Arc (PTA) process on the surface of tool steel to improve surface characteristics to improve its lifetime in working condition. The Design of Experiment (DoE) method was applied to find optimum combination of hardfacing parameters and to minimize the number of weld runs. Current, travel speed and preheat were considered as variable parameters. These parameters are important to reach a final layer with an appropriate bead geometry accompanied with good metallurgical properties. All samples were prepared for microstructural investigations and the effect of process parameters on the weld bead geometry was considered. For each weld overlay, weld bead geometry parameters were measured including dilution, penetration and reinforcement. Microstructures and the distribution of tungsten carbide particles after welding were analyzed by Scanning Electron Microscopy (SEM) equipped with an EDS microprobe. In addition, X-ray diffraction analysis was performed to find the existing phases after welding. Also, to observe the distribution of each WC in the matrix 3D optical profilometry analysis was performed. At the end, among all the experiments, the best sample with appropriate bead geometry and microstructure was selected.

**Keywords:** Design of Experiment (DoE), Hardfacing, Nickel-base powder, PTA process, Tool steel

## 1. Introduction

Hard surfacing processes lead to improve wear and corrosion properties of different components which are working in severe conditions [1–3]. By comparing different fusion welding processes, Plasma Transferred Arc (PTA) is a newly developed method with more advantages related to other conventional welding processes [3]. Some beneficial aspects of PTA process can be categorized as low heat input, high efficiency and relatively low cost. By PTA process, surface layers with high thicknesses and strong bond to the substrate can be achieved, in addition to possibility of high productivity and ability to automation mainly for weld overlay applications [1, 4, 5]. Moreover, in the PTA process, the minimum value of dilution which is an important parameter is achievable by adjusting the feeding rate [3,6]. In the PTA method, the filler material in the form of powders is carried from the powder holder to the weld pool [4]. The effect of the PTA process parameters on the microstructure and properties of the weld bead has been investigated by many researchers [7–9]. Boulithis et al. [7] studied the effect of surface treatments parameters on tool steel before and after applying heat treatment by PTA process. Nouri et al. [10] worked on the effect of the welding parameters on the properties of the hardface layer.

Chatterjee et al. [11] worked on the deposition of different layers, considering the change of welding parameters. Other authors [12–14] found that different values of these parameters leads to change the heat input and in the dilution. Moreover, their studies demonstrated that nickel-base powders used as hardfacing material can also improve the corrosion resistance of a steel product. The most widely used materials for wear resistance overlays and improving the surface properties of the substrates are nickel and iron based powder mixed with different types of carbide particles such as tungsten carbides (WC). After the deposition of the powders, the nickel matrix acts as a binder for the tungsten carbide particles. Carbides of different elements, such as tungsten, vanadium, chromium and titanium, can be mixed in different proportions to nickel-base powders and be applied on a steel product to improve its surface properties [15].

Balamurugan et al. [16] studied the optimization of the PTA process for weld overlays reinforced by TiC particles. It should be mentioned that several parameters in the PTA process, such as current, feeding rate and travel speed, have a direct effect on the quality of surface [17, 18].

Weld bead is an important geometric parameter which able to define the properties of the hardfaced layer: several studies demonstrated that there is a close relation between the weld bead shape and the quality of the layer [19–21]. Considering the different type of equipment, powder mixtures and process parameters, many combinations of the specifications could be used to find an appropriate welding procedure. To minimize this combination of parameters, it would be suggested to use the Design of Experiment (DoE) method. As a result, it is possible to decrease the number of test runs, to obtain an appropriate weld bead [16]. Ming et al. [22] and Lim et al. [23] reported effect of the feeding rate and travel speed on the quality of a nickel-based hardfacing layer applied on a low carbon steel. Palani et al. [24,25] investigated the parameter optimization for the weld overlay of stainless steel on carbon steel. Davis et al. [16] tried to find appropriate dilution and weld bead geometry by changing the process parameters. Siva et al. [26] worked on the optimization of the PTA process by using nickel-base powders on stainless steel. In addition to many investigations, still there is lack of information to find an appropriate model to predict weld bead geometry accompained with high mechanical and metallurgical properties of the layer.

Based on the DoE method, number of weld overlays with different parameters were performed on the surface of tool steel. The microstructural properties of each layer was evaluated by means of Scanning Electron Microscopy (SEM) equipped with Energy Dispersive Spectroscopy (EDS). Surface topography and detection of existing phases was performed by optical profilometer and X-ray diffraction (XRD) analysis respectively. Finally, based on the metallurgical features and the weld bead geometry measurements of the layers, the best-investigated process parameters were detected. The aim of this study was to identify the important parameters to reach good hardfaced layer of nickel base powder mixed with tungsten carbide on tool steel using PTA process. The response surface methodology was used to design the number of experiment based on different parameters. Also, in addition to metallurgical characterization of the hardfaced layers, a mathematical modeling by software was performed to predict optimal weld bead geometry.

## 2. Materials and Experimental procedure

### *2.1. Base metal and powders*

In this study, the Plasma Transferred Arc (PTA) welding process was used to apply a hardfacing layer nickel base powder on the tool steel. The tool steel in the form of a plate block with dimensions of 130 mm × 50 mm × 12.5 mm was chosen as a substrate. Before applying the hardfacing layer to the steel substrate, a specific heat treatment was performed on blocks in order to reach appropriate hardness and toughness. In particular, the blocks were preheated at 790 °C for 1 hour, then the temperature was increased to 1100 °C and maintained for 35 min [27]. The blocks were then quenched in an oil bath and subjected to two subsequent steps of tempering at 315 °C for 2 hours. After the heat treatment, oxides and possible contaminants were removed from the surfaces by smooth grinding. In this investigation, a mixture with 40 % by weight of spherical nickel-base powders and 60% of agglomerated WC particles was selected as the hardfacing material. In Table 1, the nominal chemical compositions of the base metal, nickel-base powders matrix and the WC reinforcing material are reported. The morphology of the nickel-base powders is shown in Figure 1.

Table 1. Chemical composition (wt%) of the base metal and powder

| | | Elements | | | | | | | | | | |
|---|---|---|---|---|---|---|---|---|---|---|---|---|
| | | C | Si | Cr | B | W | Ni | Mn | Mo | V | P, S | Fe |
| Base metal | | 1.58 | 0.37 | 11.53 | - | - | - | 0.48 | 0.89 | 0.56 | ≤0.03 | Bal. |
| Hardfacing powder alloy | Matrix | 0.7 | 4.5 | 15.1 | 3.2 | - | Bal. | | | | | |
| | Reinforce | 6.1 | - | - | - | Bal. | - | | | | | |

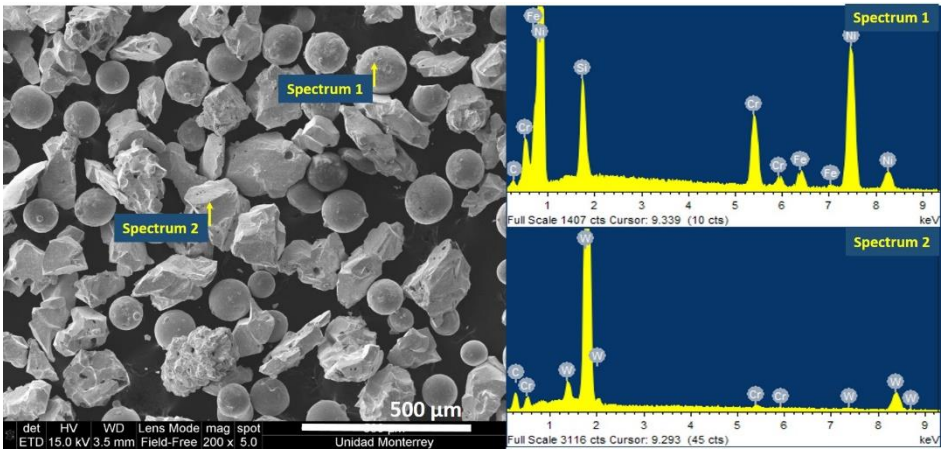


Figure 1. Morphology of the nickel-base powder mixed with WC particles

*2.2. PTA equipment and parameters*

In this investigation, the plasma machine with the Castolin Eutectic Eutronic Gap 3001DC trademark was used to apply the hardfacing layer on the tool steel plates. In the PTA process, several working parameters have to be carefully adjusted. Some of these parameters were considered as fixed and they are reported in Table 2, while current (I), preheat (T) and travel speed (S) were considered as variable. Figure 2 indicated schematic of torch of PTA equipment.

Table 2. Constant parameters of the PTA process

| Parameter | Value |
|---|---|
| Voltage (V) | 20 |
| Nozzle diameter (mm) | 3.2 |
| Torch to work piece distance (mm) | 10 |
| Plasma gas Ar (l/min) | 12 |
| Shielding gas Ar+10%$H_2$ (l/min) | 3.5 |
| Carrier gas (l/min) | 3.5 |
| Feeding rate (g/min) | 29 |

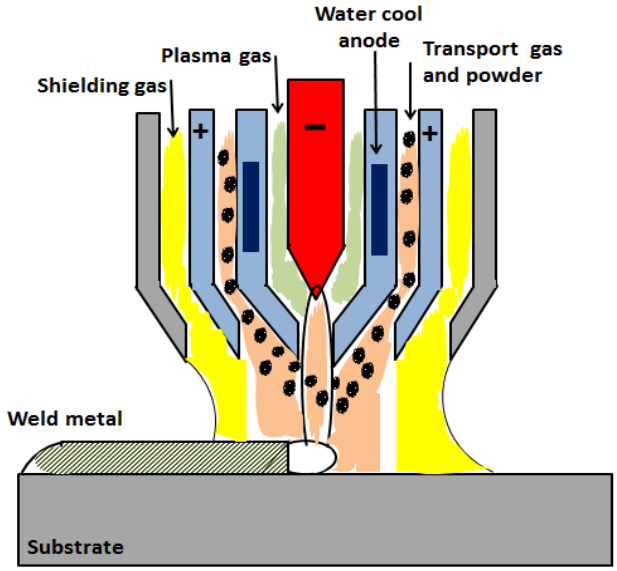


Figure 2. Schematic of the PTA process used for depositing wear resistant overlays

*2.3. Specifying the important parameters and developing the design matrix*

In PTA process, there are many variable parameters which have effect on surface layer quality, but in this investigation based on suggested important parameters and considering design of experiment (DoE) method three factors of current (A), travel speed (S) and preheat (T), with five level for each factor were considered. The reason for choosing pre heat as variable was because of susceptibility to crack initiation in tools steel during welding. Tool steel as a base metal with high carbon and high chromium percentage is sensitive to crack during welding. The design matrix chosen to perform the experiment was a central composite rotatable design. This method is useful in response surface methodology, which is a collection of statistical and mathematical methods for analyzing and modeling of engineering issues, for building a quadratic model for response variables without needing to run complete factorial level. For three factors and five levels, the required number of experimental runs is equal to $N=2^3=8$ factorials with added six center points and six star points at distance of 1.6817 units from the center points, consequently twenty runs (8+6+6=20) are required. Based on range of parameters which suggested by powder producer and literatures, the upper limit of the factor was considered as +1.6817 ($X_{\max}$) and its lower limit -1.6817 ($X_{min}$), the intermediate levels can be found as

$$X_i = 1.6817[(2X - (X_{max} + X_{min})]/(X_{max} - X_{\min}).$$

Table 3 indicates, value of parameters which were selected in this experiment.

Table 3. Variable parameters considered in this investigation

| Parameter | Notation | Factor levels | | | | |
|---|---|---|---|---|---|---|
| | | – 1.682 | -1 | 0 | +1 | +1.682 |
| Current (A) | I | 86.36 | 100 | 120 | 140 | 153.63 |
| Preheat (°C) | T | 181.82 | 250 | 350 | 450 | 518.18 |
| Travel speed (cm/min) | S | 59.7 | 70 | 85 | 100 | 110.2 |

The responses function (dilution, penetration and reinforcement) representing weld bead dimensions of one layer which is affected by value of current ($I$), travel speed ($S$) and pre heat ($T$), can be written as followed:

$Y$ is the response or Yield which is shown in equation (1)

$$Y = f(I, S, T) \qquad (1)$$

the second order polynominal (regression) equation used to represent the response surface for $K$ factors is given by equation (2)

$$Y = b_0 + \sum_{i=1}^{k} b_i X_i + \sum_{\substack{i=1 \\ i \neq j}}^{k} b_{ii} x_i \text{^} 2 + \sum_{ij=1}^{k} b_{ij} X_i X_j \qquad (2)$$

For three factors, the selected polynominal could be specified as equation (3) and (4)

$$Y = \beta_0 + \beta_1 x_1 + \beta_2 x_2 \qquad (3)$$

$$Y = (b_0 + b_i X_i + b_{ii} X_i^2 + b_{ij} X_i X_j) \qquad (4)$$

Where b0 is the free term of the regression equation. The coefficient $b_1, b_2, \dots, b_k$, are linear terms.$b_{11}, b_{22}, \dots b_{kk}$ are Quadratic term interaction terms. The coefficient $b_{12,} b_{13}, \dots, b_{k-1,k}$ are interaction terms. For three factors the selected polynominal could be expressed as equation (5)

$$Y = b_0 + b_1 * (I) + b_2 * (S) + b_3 * (T) + b_{11} * (I)^2 + b_{22}(S)^2 + b_{33} (T)^2 + b_{12}(I * S) + b_{13}(I * T) + b_{23} (S * T) \qquad (5)$$

The value of coefficient this polynominal were calculated by regression analysis with Minitab software. Also, the less important coefficient did not consider. The second order polynominal (regression equation) used to represent the response surface for $K$ factors which is given by Minitab to determine important coefficients. The final mathematical modeling for each response was determined by regression analysis as following. The adequacies of the models were tested using the analysis of variance technique (ANOVA) to study the effect of input parameters on weld bead geometry and properties. According to this technique, if the calculated value of the F-ratio of the model exceeds the standard tabulated value of F-ratio for desired level of confidence (95%), then the model may be considered appropriate within the confidence limit. It showed that the quadratic model is the best suggested model. The final models were developed using only these significant coefficients.

### *2.4. Preparation of samples*

In order to observe if there are any defects in the layers, before microstructure analysis, liquid penetrant testing was performed on the samples. All the samples were cut perpendicularly to the welding direction and a small pieces including all weld area and base metal embedded in a thermoset resin and prepared with standard metallographic procedures. An Olympus SZX A0 stereomicroscope equipped with Infinity analyze software was used for the measurements of the geometrical features of each weld layer. The schematic shape of the weld bead with indication of the most important geometrical parameters is shown in Figure 3. The values of reinforcement, penetration and dilution were measured. Microstructural analysis by Zeis EVO EMA 15 scanning electron microscope equipped with an EDS analyzer was carried out on both the base metal and the weld overlay, after chemical etching in a 2% solution of $HNO_3$ in ethylic alcohol (Nital 2) and in a solution of 70% $HNO_3$ + 30% HF, respectively.

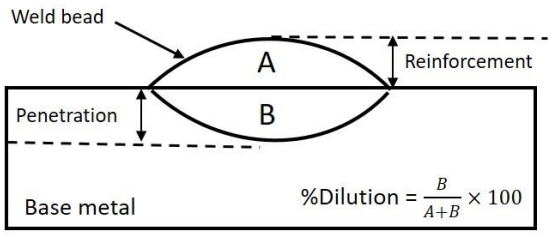


Figure 3. Schematic of weld bead geometry characteristics

## 3. Results and discussion

### *3.1. Effect of process parameters on geometry of the weld overlay*

The weld bead characteristic measurements were performed on all the samples; Table 4 indicates some of the obtained results from all twenty samples. Based on the weld bead characteristic measurements performed on the samples, Figure 4 and Figure 5 describes the effect of the travel speed and current on reinforcement and dilution respectively; in particular, when the travel speed is increased, the penetration decreases and, mainly with a travel speed of 85 and 100 cm/min, the minimum penetration values are obtained. The increase in the travel speed does not have a significant effect on dilution. When the travel speed is increased, the heat input and diffusion rate decrease; as a consequence, penetration decreases and reinforcement increases, thus keeping dilution relatively constant with just a smooth upward trend. When the current is increased, the values of penetration and dilution increase steeply, which is probably due to the increase in the heat input.

Table 4. Parameters and results of some selected samples

| Sample name | Current (A) | Travel speed (cm/min) | Preheat (°C) | Dilution (%) | Penetration (mm) | Reinforcement (mm) |
|---|---|---|---|---|---|---|
| W1 | 100 | 70 | 250 | 42.03 | 1.30 | 1.82 |
| W2 | 140 | 70 | 250 | 72.27 | 3.06 | 0.98 |
| W7 | 100 | 100 | 450 | 59.97 | 1.33 | 0.98 |
| W9 | 86.36 | 85 | 350 | 30.52 | 0.69 | 1.43 |
| W19 | 120 | 85 | 350 | 50.10 | 1.22 | 1.15 |
| W20 | 120 | 85 | 350 | 59.17 | 1.60 | 0.79 |

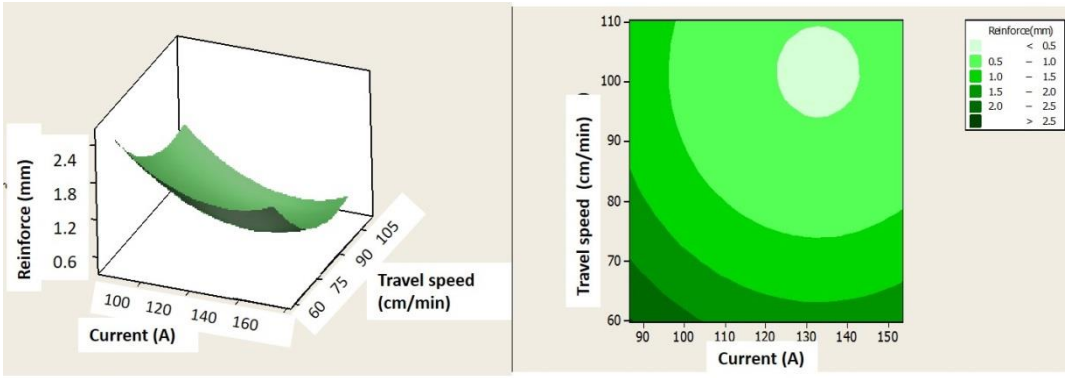


Figure 4. Effect of travel speed and current on reinforcement

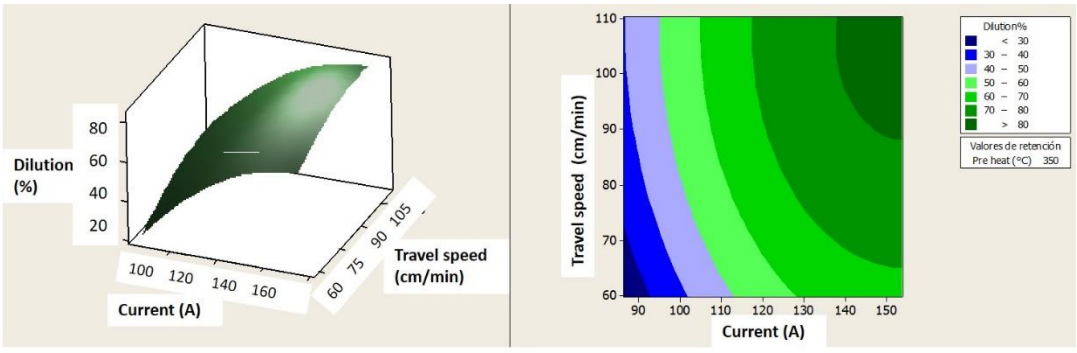


Figure 5. Effect of current and travel speed on dilution

*3.2. Microstructural characterization*

The Macro-structure of one sample cross-section observed at the stereomicroscope is shown in Figure 6a: the deposited layer, the heat affected zone and the base metal can be clearly identified in this image. The optical microscopy microstructure of different zones with relevant differences in higher magnification are visible in Figure 6b. The microstructure of the tool steel base metal, consists of predominant $Cr_{23}C_6$ which are mainly dissolved during austenization process is shown in Figure 7. The carbide structure in tempered matrix mainly related to secondary $Cr_7C_3$ secondary carbides [28]. Based on the EDX analysis existing chromium and vanadium carbides are highly detectable. VC and $V_2C$ are hard and thermally stable which leads to improve the wear and abrasion resistance of the material. The heat affected zone (HAZ) is characterized by two different microstructures close to the fusion zone and close to the base metal. The reason for the formation of these zones is probably due to the different heating and cooling rates during the hardfacing process. The relevant microstructure accompained with EDX analysis of the HAZ is shown in Figure 8.

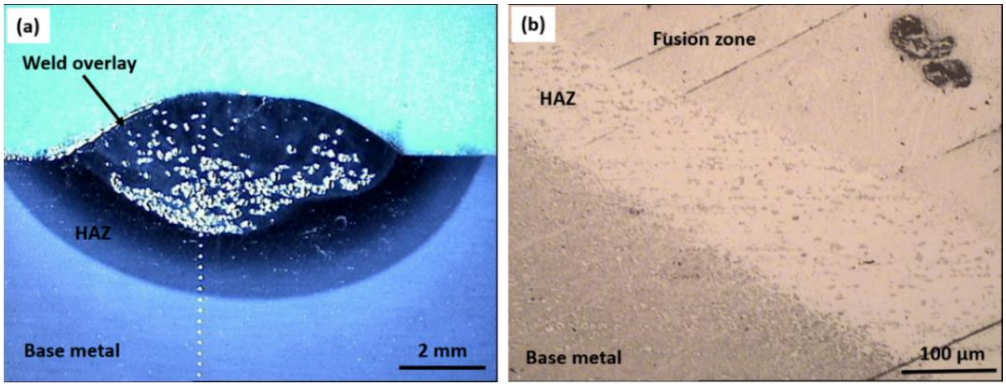


Figure 6. Macrostructure of one weld overlay

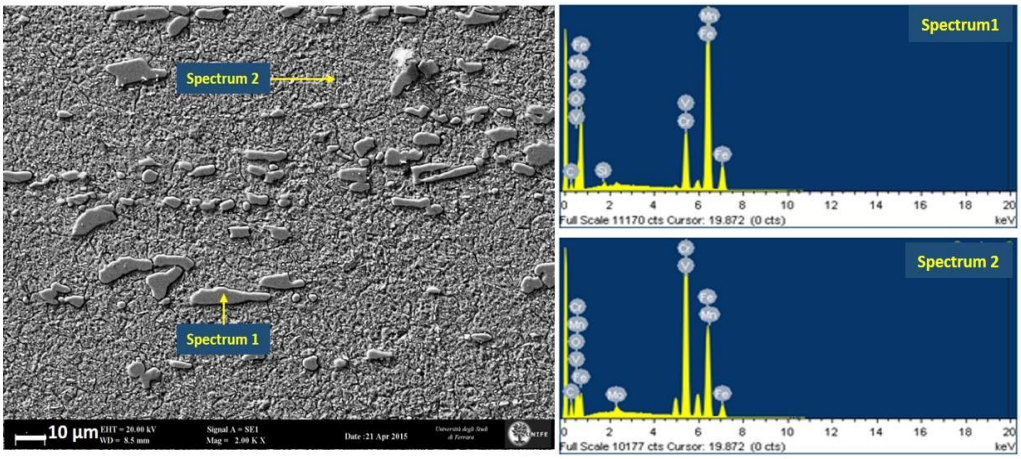


| Tool steel | C | Si | V | Cr | Mn | Fe |
|---|---|---|---|---|---|---|
| Spectrum 1 | 11.54 | - | 3.89 | 44.27 | 0.4 | Bal. |
| Spectrum 2 | 6.13 | 0.46 | 0.64 | 13.80 | 0.51 | Bal. |

Figure 7. Microstructure of the base metal

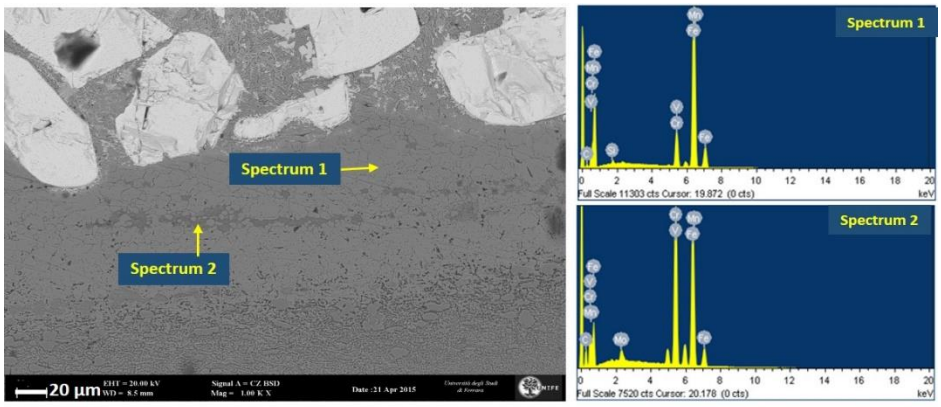


| HAZ | C | Si | V | Cr | Mn | Mo | Fe |
|---|---|---|---|---|---|---|---|
| Spectrum 1 | 4.08 | 0.66 | 0.47 | 10.45 | 0.34 | - | Bal. |
| Spectrum 2 | 12.46 | - | 2.91 | 33.72 | - | 2.62 | Bal. |

Figure 8. Microstructure of the heat affected zone and EDX analysis of phases

The SEM micrographs of a nickel-based hardfacing layer in different magnifications is shown in Figure 9. The microstructure can be characterized by a γ-Ni primary hypereutectic dendritic phase and a lamellar eutectic structure in the interdendritic regions [29]. Irregular blocky-shaped tungsten carbide particles are distributed in the nickel matrix and are clearly visible in Figure 9a and b. Also the dendritic microstructure of nickel matrix in high magnifications can be observed in Figure 9c.

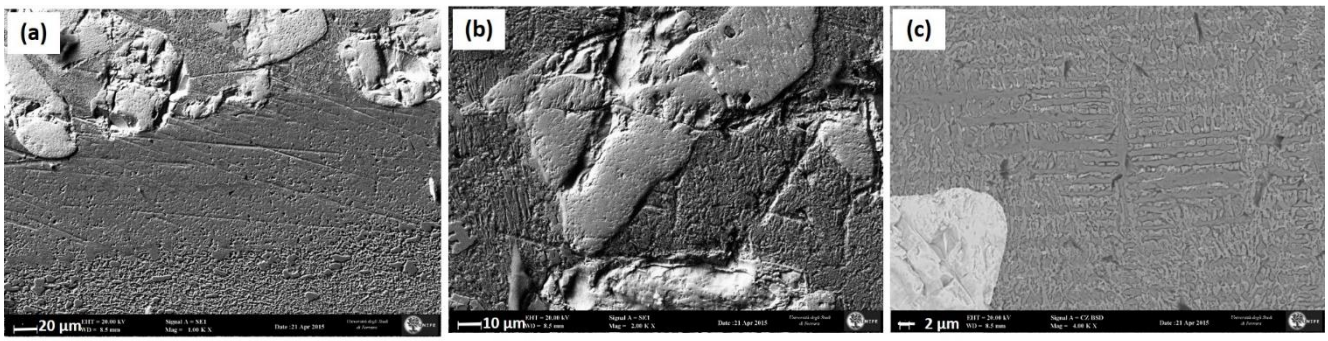


Figure 9. Microstructure of the weld overlay: (a) WC particles close to base metal, (b) WC in high magnifications and (c) dendritic nickel matrix

### *3.3. Distribution of Tungsten carbides in the matrix*

The distribution of tungsten carbides in the layers were not completely uniform and homogeneous as it shown in Figure 10, also mainly they were accumulated at the bottom of the weld bead near to the base material. It is due to their high density; the volume fraction of tungsten carbides close to the top surface of the layer is lower than in the area at the bottom of the weld pool close to the substrate.

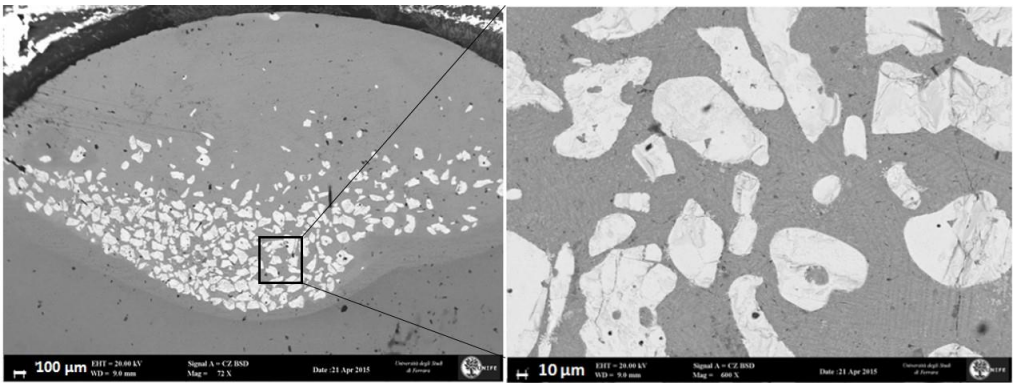


Figure 1. Distribution and morphology of tungsten carbides at the bottom of the layer

Figure 11 shows the cross-sections of some selected layers obtained from image analyser software to observe the distribution of WC in the weld bead. As can be seen, sample W9 and W19 show more regular weld bead geometry and a more homogenous distribution of tungsten carbides and these particles are better distributed through the weld bead area. For most of the other samples, tungsten carbide particles are preferentially distributed at the bottom of the weld pool. Moreover, different samples present different values of penetration and reinforcement due to the different process parameters. The interface between WC and Ni matrix was fine but in some cases pores were form close to the WC particles. Generally, the hardness of WC is very high and it is difficult to grinding with emery papers, during grinding, some part of carbides was worn and stick to the emery papers, in this case the papers acts as abrasive material, consequently pits and ducts forms on the carbide particles. Also, based on previous research in case of increasing the current, there is possibility of the changing WC phase to W2C phase which is more brittle than WC. [30, 31].

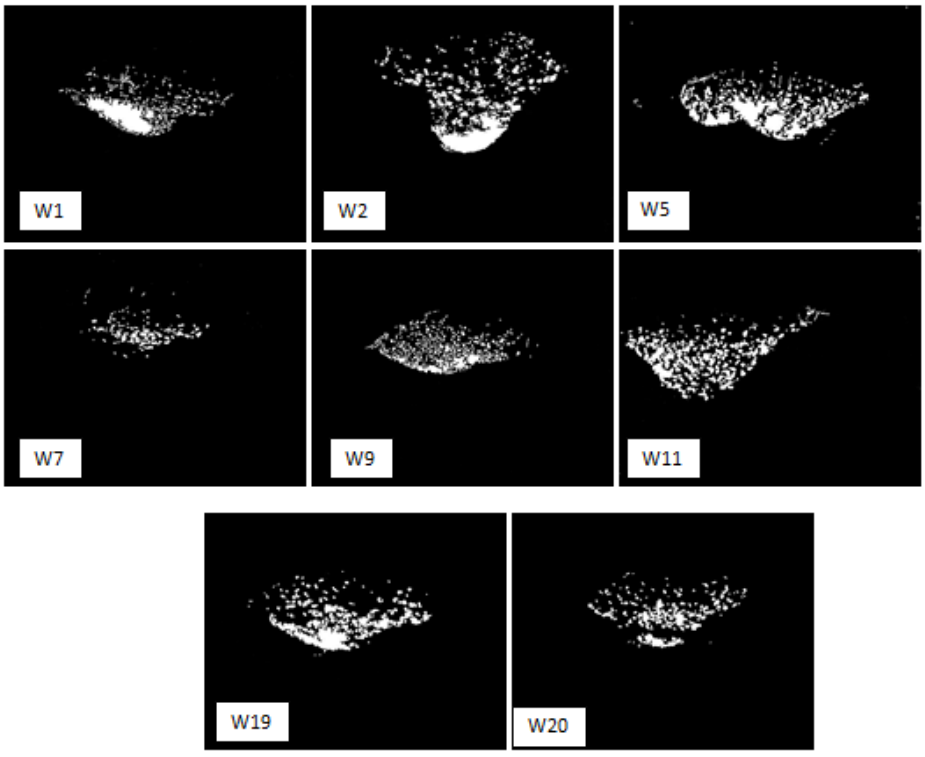


Figure 11. Distribution of WC particles at the bottom of the weld pool

In addition, based on calculation of image analyzer, the percentage of tungsten carbide in the weld pool was measured and the relevant results are listed in Table 5. As it is clear, mainly this percentage for most of the samples are between 30 to 45%, which is appropriate value.

Table 5. Percentage of WC in some selected samples

| Sample | W1 | W2 | W5 | W11 | W19 | W20 |
|---|---|---|---|---|---|---|
| % WC in matrix | 33.65 | 30.36 | 43.02 | 45.04 | 38.62 | 34.28 |

### *3.4. SEM and EDS analysis*

Back scattered images of the deposited layer, obtained by means of SEM from one sample is reported in Figure 12. To observe the distribution of alloying elements in the matrix, EDS analysis was performed on different in different parts of the microstructure, the results are shown in Table 6. In addition to large tungsten carbides, there are other different intermetallic phases containing nickel, chromium and silicon, distributed between matrix and WC particles. The diffusion of interstitial carbon in the matrix is faster than other carbide former elements; in the presence of WC as a reinforced material, the formation of other complex and brittle carbides was reported in the literature [32]. EDX analysis of the carbides indicates that, in addition to chromium, there is possibility of existing vanadium to form carbide and distributed in the matrix. From the results, it can be observed that tungsten is also distributed in the matrix about 15%. This could be due to decarburization of $WC/W_2C$ during the welding process; moreover, tungsten and carbon could be dissolved into the nickel and nickel-chromium phases. Dissolution of tungsten carbide particles in the matrix causes the precipitation of secondary carbides around the primary ones.

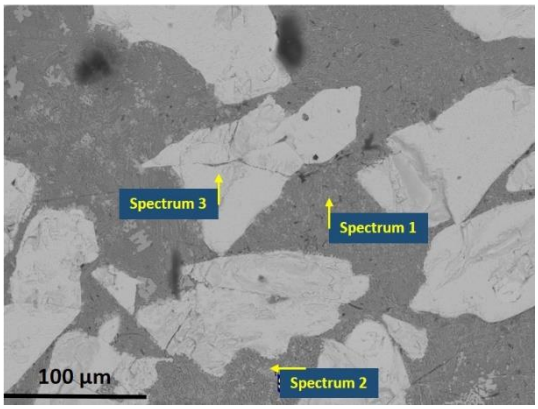


Figure 12. SEM micrograph of WC in the matrix and position of EDX analysis EDS analysis

Table 6. Qualitative data (wt%) of EDX analysis

| | Position | C | W | Si | V | Cr | Fe | Ni |
|---|---|---|---|---|---|---|---|---|
| Spectrum 1 | Matrix | 2.78 | 15.24 | 2.56 | - | 5.61 | 37.33 | 36.48 |
| Spectrum 2 | Carbide/Matrix | 5.01 | 50.86 | 3.15 | 0.37 | 13.70 | 9.21 | 17.70 |
| Spectrum 3 | Carbide | 7.24 | 92.76 | - | - | - | - | - |

Figure 13 indicates the EDX map analysis of the elements in cross section of the layer. It is clear that tungsten and silicon are the main elements in large particles, also distribution of Ni, Cr and Fe elements in matrix are uniform and homogeneously distributed.

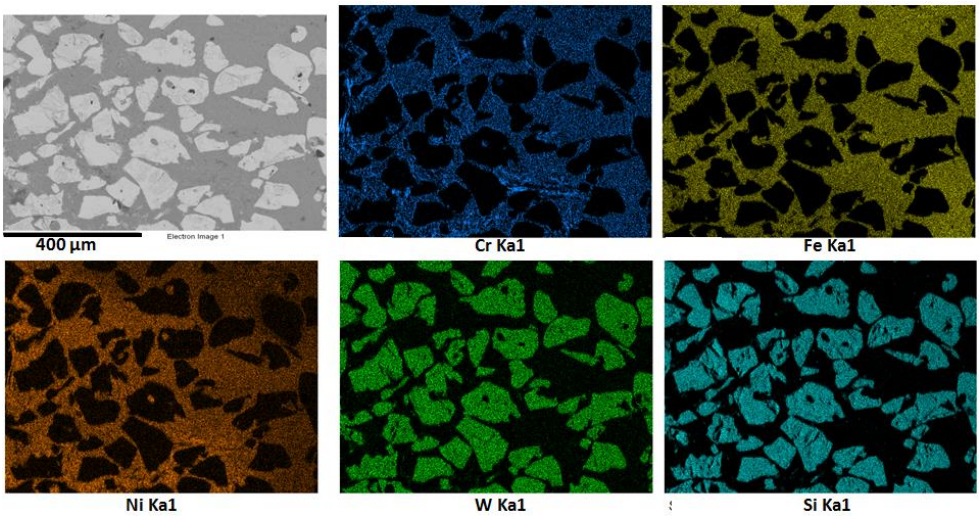


Figure 13. Distribution of elements in weld layer

### *3.5. X-ray diffraction*

Figure 14, shows the obtained X-ray spectrums from the one welded sample. The main phases formed in optimized sample are $W_2C$, WC, $Cr_3Si$, $Ni_2B$ and NiCrFe. As it is clear tungsten carbide is formed in two forms of $W_2C$ and WC. Based on peak intensity value, the amount of $W_2C$ is less than WC. The main peak intensity in the matrix is related to NiCrFe phase. It is important to mention that WCrC phase in the microstructure is not possible to observe which is due to its location close to the bottom of the weld bead and low percentage of this phase in the microstructure.

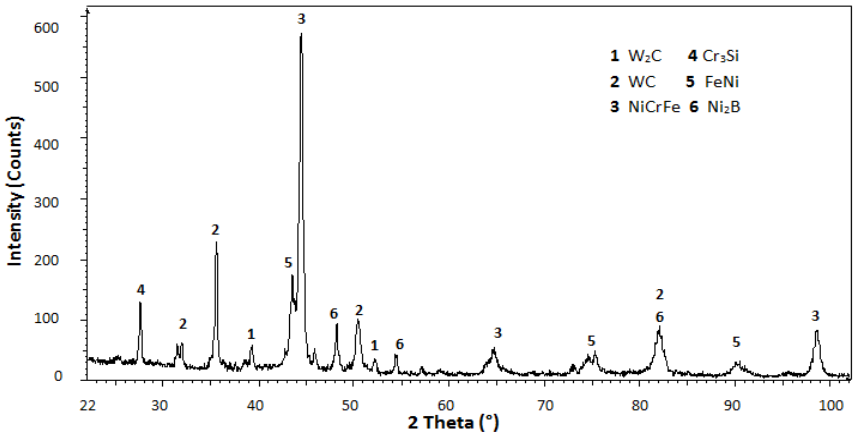


Figure 14. XRD spectrum of the optimized sample

### *3.6. Surface optical profilometry*

Surface profile analysis was performed by means of optical profilometer in two and three dimensions. Based on obtained data maximum differences between matrix and tungsten carbides are around 9µm. Also, 3D profile of the sample in Figure 15 indicates the distribution and height of the tungsten carbide on matrix. Figure 16 indicated 3D and 2D surface profile of one single tungsten carbide in the matrix accompanied with one-line scan profile between two points. As it is visible, there is differences between height of tungsten carbide and matrix even if after metallographic preparation. 2D profile line scan specified that for one single tungsten carbide particle is about one micron higher than reference line of interface, but the maximum height differences reach to 3.5 micron. Also based on intrinsic irregular morphology of tungsten carbide, some holes and voids on the particles and interface of particles and matrix are visible.

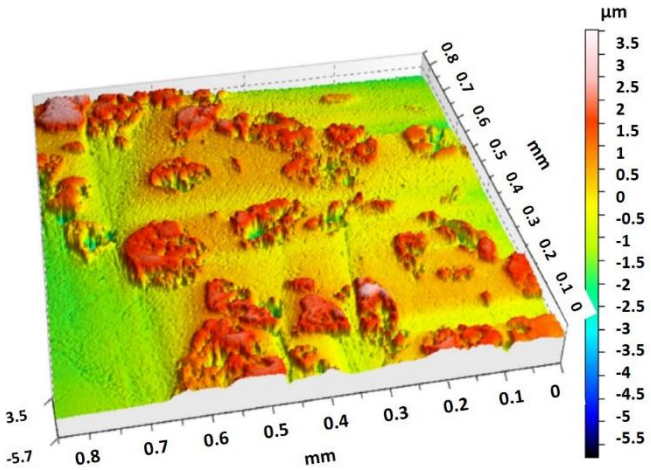


Figure 15. 3D surface profile of distribution of tungsten carbide

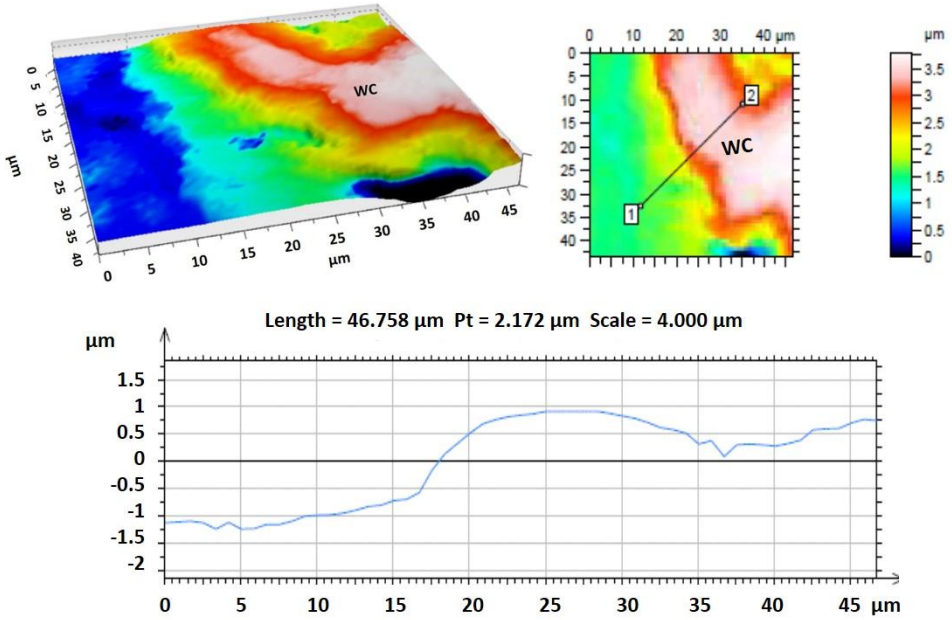


Figure 16. Profile of a single tungsten carbide in matrix (a)3D (b)2D (c) surface profile between two pints

### *3.7. Weld bead geometry and optimization of the process*

Considering the weld bead geometry parameters, the distribution of tungsten carbides and surface profilometry the quality of sample W9 can be considered the optimum compared to other samples. The process parameters and the weld bead geometry results for the optimum experimental sample and optimum prediction by modelling is specified in Table 7. Nevertheless, considering the several possible sets of process variables, it is relatively difficult to find the best welding parameters to predict and reach appropriate weld bead characteristics. Based on what is suggested in the literature [5, 10, 26, 33], to reach appropriate weld layer geometry, the value of reinforcement should be the maximum, while the values of penetration and dilution should be the minimum. It is very important to select appropriate process parameter to obtain optimal weld bead geometry [10] and [33]. To find the optimum parameters, there are many optimization methods [34], which needs more in depth mathematical investigation, but according to optimization of the parameters with using the multiple objectives, it is possible to obtain optimum parameters which can be obtained by Minitab software. As can be seen, the parameters obtained from the model is relatively close to the sample W9, just there is a little change in the value of penetration. Also, the obtained optimum data by modeling should be validated experimentally.

Table 7. Parameters and results of optimum experimental sample

| Sample name. | Current (A) | Travel speed (cm/min) | Preheat (°C) | Dilution (%) | Penetration (mm) | Reinforcement (mm) |
|---|---|---|---|---|---|---|
| W9 | 86.36 | 85 | 350 | 30.52 | 0.69 | 1.43 |
| Optimum by model prediction | 86 | 60 | 225 | 36.84 | 1.38 | 1.80 |

## 4. Conclusions

In this study a powder consists of nickel matrix reinforced by tungsten carbide particles was applied on the tool steel by Plasma Transferred Arc (PTA) process. To reach optimum weld bead geometry accompained with appropriate metallurgical properties, a combination of different process parameters (current, travel speed and preheat) by using design of experiment (DOE) method were considered. After characterization of the samples the following conclusions can be drawn:

- Design of experiments was a useful method to investigate the effect of process parameters on the weld bead geometry in the PTA process. When the current, penetration and dilution increase, the reinforcement decreases. By increasing the travel speed, penetration decreases, dilution mainly remain constant with a slight increase. The current was the most important process parameter which had strong effect on the geometry of the weld and the distribution of the carbides.
- The WC particles was not homogeneously distributed in the weld pool and mainly accumulated at the bottom of the layer close to the base metal. Among all conditions just for two sets of parameters these carbides in the matrix were well distributed.
- Analysis by SEM and EDX on the samples indicated that, in addition to WC particles, tungsten was dissolved in the nickel matrix. Complex phases containing tungsten and other carbides former elements were detected in the layers.
- Results of surface profilometry showed that, in addition to well surface preparation, still there is inhomogeneity between the height of the WC and nickel matrix.
- From the microstructural and geometrical data obtained from the analyzed samples, the optimum parameters for hardfacing were actually found as: current 86.36 A, travel speed 85 cm/min and preheat 350 °C. With these parameters, the values of dilution, penetration, reinforcement and bead width were 30.52%, 0.69 mm, 1.43 mm and 6.53 mm, respectively. It is very difficult to find the optimum parameters to obtain high quality weld bead geometries. The obtained model proposed that with choosing the parameters of 86 A current, 60 cm/min travel speed and 225 °C preheat the dilution 36.84 %, penetration and reinforcement will be 1.38 and 1.80 mm respectively. These parameters practically should be validated.

## Acknowledgements

Ali Tahaei gratefully acknowledges IUSS 1391 of the University of Ferrara (Unife) for its financial support. Special thanks should also be given to CONACYT for both its financial and experimental support during the internship at Corporación Mexicana de Investigación en Materiales (COMIMSA). The PTA process was performed at Cimav.

## References

[1] E. Gruzdys, S. Meskinis, Influence of Plasma Transferred Arc Process Parameters on Structure and Mechanical Properties of Wear Resistive NiCrBSi-WC/Co Coatings, Materials Science (MEDZIAGOTYRA), v.17, n.2, p.140–144, 2011.

[2] V. Vergaradiaz, J. Carlos Dutra, A.S. Climaco D'oliviera, Hardfacing by Plasma Transferred Arc Process, www.intechopen.com.

[3] R.L. Deuis, J.M. Yellup, C. Subramanian, Metal-Matrix composite coating by PTA surfacing, Composite Science and Technology, v.58, p. 299–309, 1998.

[4] J.R. Davis, Davis & Associates, Metals Handbook, Hardfacing, Weld Cladding and Dissimilar Metal Joining ASM Handbook: Welding, Brazing and Soldering. 10th Ed., ASM Metals Park, OH, 6: p. 699–823, 1993.
[5] V. Balasubrarnian, A.K. Lakshminarayan, R. Varahamoorthy, Application of Response Surface Methodology to Prediction of Dilution in Plasma Transferred Arc Hardfacing of Stainless Steel on Carbon Steel, Journal of Iron and Steel research, International, v.16, n.1, p. 44–53, 2009.
[6] K. Siva, N. Murugan, A Study on the Influence of PTAW Process Parameters on Pitting Corrosion Resistance of Nickel Based Overlays, Procedia Engineering, v.64, p. 1147–1156, 2013.
[7] E. Bourithis, A. Tazedakis, G. Papadimitriou A study on the surface treatment of "Calmax" tool steel by a plasma transferred arc (PTA) process, Journal of Materials Processing Technology, v.128, p.169–177, 2002.
[8] C. Sudha, P. Shankar, R.V. Subba Rao, R. Thirumurugsan, M. Vijayalakshmi, B. Raj, Microchemical and microstructural studies in a PTA weld overlay of Ni–Cr–Si–B alloy on AISI 304L stainless steel, Surface & Coatings Technology, v.202, p.2103–2112, 2008.
[9] H.J. Kim, B.H. Yoon, C.H. Lee, Wear performance of the Fe-based alloy coatings produced by plasma transferred arc weld-surfacing process, Wear, v.249, p. 846–852, 2002.
[10] M. Nouri, A. Abdollah zadeh, F. Malek, Effect of Welding Parameters on Dilution and Weld Bead Geometry in Cladding, Journal of Material Science Technology, v.23, n.6, p. 817–822, 2007.
[11] S. Chatterjee, T.K. Pal, Wear behaviour of hardfacing deposits on cast iron, Wear, v.255, p.417–425, 2003.
[12] D. Kesavan, M. Kamaraj, The microstructure and high temperature wear performance of a nickel base hardfaced coating, Surface & Coatings Technology, v.204, p. 4034–4043, 2010.
[13] C.S. Ramachandran, V. Balasubramanian, R. Varahamoorthy, Evaluation of Dry Sliding Wear Behaviour of Plasma Transferred Arc Hardfaced Stainless Steel, International Journal of Iron and steel research, v.16, n.4, p.49–54, 2009.
[14] A. Zikin, I. Hussainova, C. Katsich, Advanced chromium carbide-based hardfacing, Surface & Coatings Technology, v.206, p.4270–4278, 2012.
[15] A. E. Yaedu, A. S. C. M. D'oliviera, Cobalt based alloy PTA hardfacing on different substrate steels, Materials Science and Technology, v.21, n.4, p.459–466, 2005.
[16] S. Balamurgan; N. Murugan, Design of Experiment and Optimization of Plasma Transferred Arc Hardfacing on Structural Steel with Titanium Carbide, Research Journal of Applied Sciences, Engineering and Technology, v.7, n.11, p.2362–2370, 2014.
[17] A. Conde, F. Zubiri, Y.J. De damborenea, Cladding of Ni–Cr–B–Si coatings with a high power diode laser, Materials Science and Engineering A, v.334, p.233–238, 2002.
[18] M.J. Tobar, C. Alvarezi, J.M. Amado, Morphology and characterization of laser clad composite NiCrBSi–WC coatings on stainless steel, Surface & Coatings Technology, v.200, p.6313–6317, 2006.
[19] J.C. Mc Glone, Weld bead geometry prediction – a review, Metal Construction, v.14, p.378–384, 1982.
[20] F. Garcia Vazquez; AGUIRRE, A. Arizmendi, Analysis of weld bead parameters of overlay deposited on D2 steel components by plasma transferred arc (PTA) process, Materials Science Forum, v.755, p. 39-45, 2013.
[21] I-S. Kim; J-S. Son, Y-J. Jeung, Control and optimization of bead width for multi-pass welding in robotic arc welding processes, Austrian Welding Journal, v.46, p. 43–46, 2001.
[22] Q. Ming, L.C. Lim, Z.D. Chen Laser cladding of nickel-based hardfacing alloys, Surface and Coatings Technology, v.106, p.174–182, 1998.
[23] L.C. Lim, Q. Ming, Z.C. Chen Microstructures of laser-clad nickel-based hardfacing alloys, Surface and Coatings Technology, v.106, p.183–192, 1998.
[24] P.K. Palani, N. Murugan, Optimization of weld bead geometry for stainless steel claddings deposited by FCAW, Journal of Materials Processing Technology, v.190, p.291–299, 2007.
[25] P.K. Palani, N. Murugan, Development of mathematical models for prediction of weld bead geometry in cladding by flux cored arc welding, International Journal of Advanced Manufacturing Technology, v.30, p.669–676, 2006.
[26] K. Siva, N. Murugan, V.P. Raghupathy, Modelling, analysis and optimization of weld bead parameters of nickel based overlay deposited by plasma transferred arc surfacing, Computational Materials Science and Surface Engineering, v.1, n.3, p.174–182, 2009.
[27] H.E. Chandler; Heat Treater's Guide: Practices and Procedures for Irons and Steels, ASM international, 1994
[28] ROBERTS, G. Tool steels. 5th ed. ASM, International; 1998.
[29] J. W. Fu, Y. S. Yang and J. J. Guo, Microstructure selection of Fe–Cr–Ni alloy during directional solidification, International Journal of Cast Metals Research, v.23, n.2, p.119–123, 2010.
[30] V. Stoica, R. Ahmed, T. Itsukaichi, Influence of heat-treatment on the sliding wear of thermal spray cermet coatings, Surface & Coatings Technology, v.199, p.7-21, 2005
[31] M.F. Morks, G. Yang, N.F. Fahim, F.U. Yingqing, Microstructure and hardness properties of cermet coating sprayed by low power plasma, Materials Letters, v.60, p.1049-1053, 2006.
[32] Q. Li, T.C. Lei, W.Z. Chen, Microstructural characterization of WC reinforced Ni–Cr–B–Si–C composite coatings, Surface and Coatings Technology, v.114, p285–291, 1999.

[33] E. Bhaskarananda Dasgupta, S. Mmukherjee, Optimization of Weld Bead Parameters of Nickel Based Overlay Deposited by Plasma Transferred Arc Surfacing, International Journal of Modern Engineering Research (IJMER), v.3, n.3, p.1330-1335, 2013.
[34] D.S. Nagesh, G.L. Datta, Prediction of weld bead geometry and penetration in shielded metal-arc welding using artificial neural networks, Journal of Materials Processing Technology, v.123, p. 303–312, 2002.

ICSE-Q
1st International Congress on Surface Engineering
IWTS-Q

June 29th-
July 1st
2016

CONACYT CENAPROT CIATEQ CIDESI Cinvestav

This is to certify that, the contribution entitled

# Influence of tungsten carbide nano-crystal particle addition on the hardfacing properties of nickel-based

by

Ali Tahaei, Paul Horley, David Torres-Torres, Gian Luca Garagnani, H. Siller, A. Arizmendi-Morquecho

has been presented in the 1st International Congress on Surface Engineering
Querétaro - México. June 29th - 30th, 2016.

Juan Muñoz Saldaña, Dr. Ing.
Organizing Committee Director

Querétaro, Qro. México

ICSE-Q
1st International Congress on Surface Engineering
IWTS-Q

June 29th-
July 1st
2016

CONACYT CENAPROT CIATEQ CIDESI Cinvestav

# Certificate of Participation

To: ARIZMENDI ANA

For attending the 1st International Congress on Surface Engineering
Querétaro - México, June 29th - July 1st, 2016.

Juan Muñoz Saldaña, Dr. Ing.
Organizing Committee Director

Querétaro, Qro. México